Plasma Chem Plasma Process
DOI 10.1007/s11090-016-9758-6

ORIGINAL PAPER

Quantum Chemical Approach for Determining Degradation Pathways of Phenol by Electrical Discharge Plasmas

Xiangru Fan[1] · John B. McLaughlin[1] · Artem Melman[2] · Selma Mededovic Thagard[1]

Received: 6 March 2016 / Accepted: 27 October 2016

Abstract This study uses density functional theory (DFT) simulations to predict the main pathways by which hydroxyl (OH) radicals oxidize phenol into monohydroxylated products during an electrical discharge directly in or contacting water. The calculated activation energies and reaction rate constants indicate that phenol ring H abstraction is less likely to occur than OH addition, which will be the fastest in the *ortho* and *para* positions. The chain propagation with molecular oxygen of such formed *ortho* and *para* radicals will result in the production of hydroquinone and catechol, which are, concurrently, the most likely products of phenol degradation by OH radicals. Electron transfer reactions between dihydroxycyclohexadienyl radicals and plasma oxidative species are another important reaction mechanism which may be contributing significantly to the formation of products. Good agreement between computed kinetic and experimental data demonstrates the feasibility of applying DFT to investigate chemical reaction mechanisms.

Keywords Density functional theory · Electrical discharge · Phenol · Plasma

Electronic supplementary material The online version of this article (doi:10.1007/s11090-016-9758-6) contains supplementary material, which is available to authorized users.

✉ Selma Mededovic Thagard
smededov@clarkson.edu

[1] Plasma Research Laboratory, Department of Chemical and Biomolecular Engineering, Clarkson University, 8 Clarkson Avenue, Potsdam, NY 13699, USA

[2] Department of Chemistry, Clarkson University, 8 Clarkson Avenue, Potsdam, NY 13699, USA

Published online: 19 November 2016

Introduction

Electrical discharge plasmas are under extensive investigation for numerous applications including gas cleaning, chemical syntheses, surface modification, and, more recently, plasma sterilization and plasma medicine. Since the discovery that OH radicals, which are formed by electronic (and in some cases thermal) splitting of water molecules, degrade organic compounds, electrical plasmas formed directly in and contacting water have also been investigated as an alternative advanced oxidation technology (AOT) for drinking and wastewater treatment. Some studies suggest that apart from OH radicals other reactive species such as H, O, and HO_2/O_2^- radicals, H_2O_2, O_2, and aqueous electrons (e_{aq}^-) also degrade organic molecules [1, 2]. However, experimental evidence for the plasma-assisted degradation of organic molecules by reactive radicals other than OH is scarce. This is, in part, due to the lack of experimental techniques available for scavenging and detecting radical species in aqueous plasmas as well as the non-selectivity of the existing chemical probes.

Computer simulations represent an alternative approach to studying the likelihood of a broad range of degradation pathways a parent compound might undergo upon reacting with different radicals [3–6]. In addition, recent developments in the field of computational chemistry have given rise to several novel computational methods that can deliver a dramatically improved accuracy without a significant increase in computational cost. However, although there are ample high quality computational studies on chemical kinetics involving different radicals and organic molecules [7–12], only a few of them apply to chemical reactions occurring in aqueous electrical discharge plasmas.

In this study, DFT simulations were used to elucidate the main pathways by which OH radicals chemically transform phenol. Though the calculations were primarily intended to apply to reactions of electrical discharge plasmas formed directly in and contacting water at the plasma-bulk liquid interface where the temperature is assumed to be 298 K, the chemical reaction mechanisms identified in this study are applicable to any AOT including, but not limited to, Fenton's reaction and sonochemistry. Phenol was chosen as a model compound due to a wide availability of experimental data, relatively well known degradation reaction pathways, and the environmental importance of its oxidative degradation. Phenol is an important raw material in the production of phenolic resins, caprolactam and bisphenol A. The latter two compounds are intermediates in the manufacture of nylon and epoxy resins, respectively. The Environmental Protection Agency regulates phenol under the Clean Water Act. Phenol has been used as a model compound for the evaluation of many water treatment technologies including electrical discharge plasma. In fact, phenol is one of the most studied compounds for the assessment of the effectiveness of different electrical discharge plasma reactors in pollutant removal.

While the complete oxidation of phenol by OH radical attack yields organic and inorganic acids, due to the complexity and lengthiness of the overall mechanism, this study considers only the first steps in which phenol is transformed into monohydroxylated products such as catechol (CA), hydroquinone (HQ), and resorcinol (RS). The subsequent paper, which is in preparation, investigates further reactions of OH radicals with CA, HQ, and RS as well as reactions of phenol with H radicals and electrons. The database of chemical reactions between phenol and OH radicals was constructed using reaction mechanisms and products identified in Fenton chemistry [13–20], atmospheric chemistry [21–25], photocatalysis [19, 26–32], radiation chemistry [31, 33–35], electrochemistry [36–39], as well as plasma chemistry studies [20, 26, 40–54]. Reaction rate constants at

298 K for individual reactions were also calculated and, when possible, compared with experimental and other DFT computational studies data.

Computational Protocols

Geometries and frequency analyses were computed using the Gaussian 09 D.01 program [55]. All the geometries, unless otherwise specified, were optimized and transition states located using the 6-31G+(d,p) basis set [56] and M062X functional [57] with unrestricted formalism and ultrafine integration grid. The accuracy of this protocol was confirmed by comparing the obtained geometries with geometries found in a previously published study [10]. The solvation effect was taken into account by using the polarizable continuum model (PCM) with SCRF = IEF-PCM keyword [58]. Vibrational frequencies and the thermal contribution to Gibbs free energy and enthalpy were also calculated at this level.

Final single point energy calculations, unless otherwise specified, for both stable species and transition states were performed with the ORCA software [59] using the PWPB95 [60] density functional with unrestricted formalism and integration grid level 5 and the ma-def2-TZVPP basis set [61]. The solvent effect was modeled using the more accurate SMD solvation model, which was most likely the largest source of error for the chosen calculation protocol [62]. According to a benchmark study conducted by Goerigk and Grimme [63], the mean absolute deviation for barrier height of hydrogen abstraction reaction for PWPB95 density functional is as low as 1.8 kcal/mol. The mean unsigned error for SMD solvation model is 0.6–1.0 kcal/mol for neutral species [62], so the reaction Gibbs free energies calculated in this study should be highly reliable. However, for reactions occurring in liquid water, the use of an implicit solvation model may be inadequate to describe the involvement of water clusters in the transition state, hence affecting the accuracy of the computed barrier height. Despite all the drawbacks of the implicit solvation model, it is nevertheless the only feasible modeling method one can choose for such a large-scale reaction kinetic study [64]. Density fits were enabled for both the SCF exchange part and the perturbation part using RIJCOSX and RI-PWPB95 keywords. For reactions in which the described calculation protocol did not converge, the 6-311+G(d,p)/M062X//midix/M062X protocol was used.

All transition states (TS), unless otherwise specified, were located using the Berny algorithm [65] with the following keyword, opt = (ts, calcfc, noeigen) under the same calculation protocol as the geometry optimization. Initial guesses for transition state geometry were generated by the plasma chemistry database system software developed by our research group. When the Berny algorithm failed or the geometry was too complex to envisage a suitable initial guess, the QST2 and QST3 methods [66] were used to attain the transition state. Transition states were confirmed by checking the direction of the negative mode of the vibrational frequencies. For suspicious transition states, an intrinsic reaction coordinate (IRC) calculation was conducted to confirm the transition state.

The plasma chemistry database system software was used to compute reaction rate constants with transition state theory (TST) and the Wigner tunneling correction [67]. Although both TST and Wigner tunneling correction calculations are theoretically very crude, they have the advantage of being computationally straightforward and are able to deliver qualitatively correct rate constants. The activation energy reported in this paper is derived from the Eyring equation and is equal to the change in enthalpy between the transition state and reactants. The electrode potentials E were calculated from the change in

reaction Gibbs free energy ($\Delta_r G = -nFE$ where n is the number of electrons transferred and F is the Faraday constant). The electrode potential calculated using this approach was scaled with respect to $E_{H+/H2}$, which was set to zero.

Results and Discussion

Phenol reaction with OH radicals can proceed via two general pathways shown in Fig. 1: OH radical abstraction of an H atom (path X) or OH radical addition to the phenol ring (path Y). Both pathways yield intermediate radicals which either recombine (paths X.A and Y.A) or chain propagate (paths X.B, Y.B, Y.C, and Y.D) to form stable molecules. Sections 3.1 and 3.2 provide mechanistic details for each of these pathways and use thermodynamic and kinetic data to determine the most probable reactions.

Path X: Abstraction of an H Atom

The OH radical abstraction of the phenolic H atom results in the formation of phenoxyl radical (PXR), as shown in reaction 1.

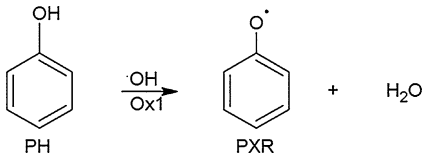

(1)

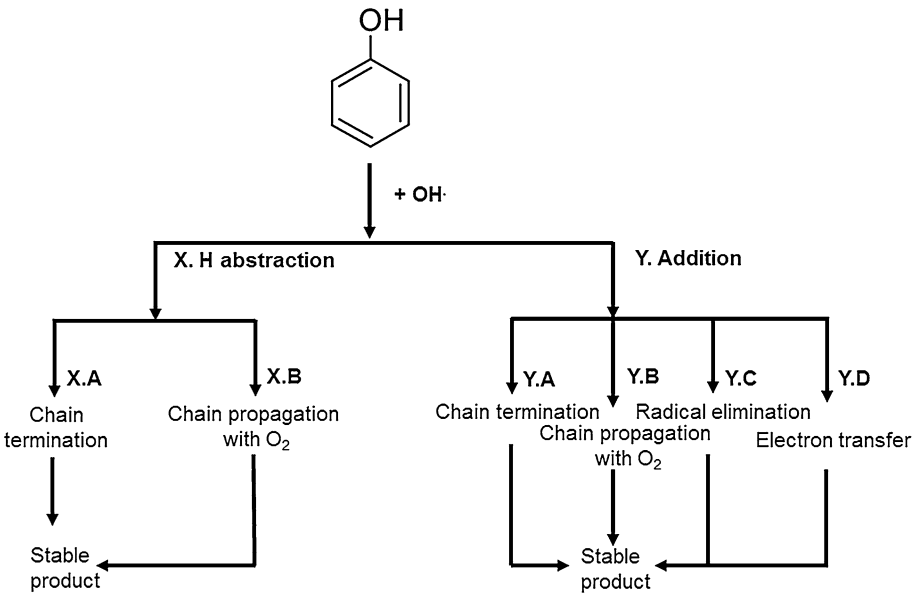

Fig. 1 An overview of the types of chemical reactions phenol undergoes upon OH radical attack

The abstraction of the H atom bonded to the second, third, and fourth phenol carbon atom yields PH2DHR, PH3DHR, and PH4DHR radicals respectively:

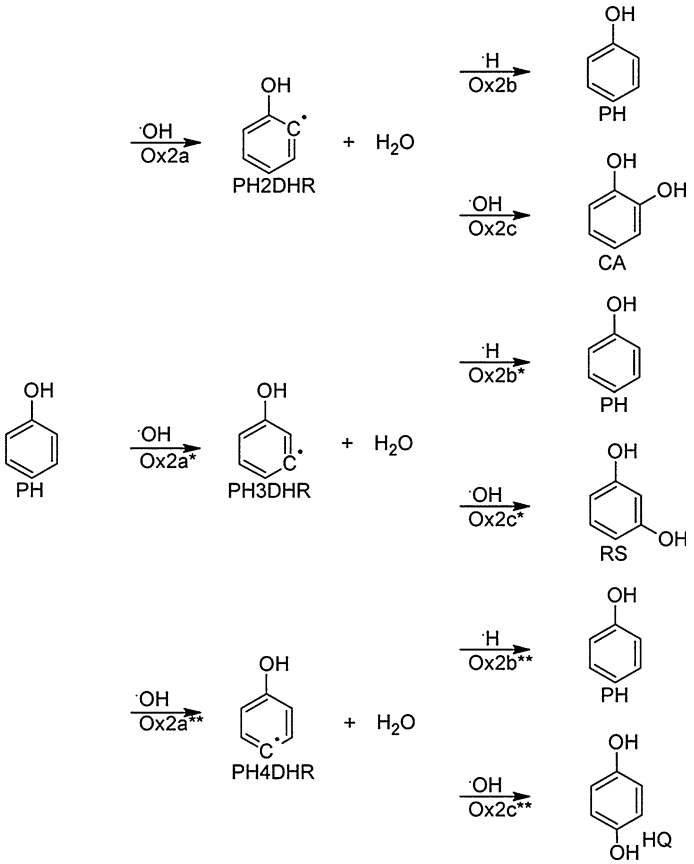

(2)

All these radicals, including PXR, may undergo further reactions with OH and H radicals, the most abundant radical species produced by aqueous plasmas to form stable products (path X.A in Fig. 1). It must also be mentioned that HO_2 radicals can recombine with any organic intermediate radical to form organic peroxides. However, due to the complexity of the reactions involving organic peroxides, recombination reactions of HO_2 and organic radicals were not included in the analysis. The recombination reactions of PH2DHR, PH3DHR, and PH4DHR with OH and H radicals may yield PH, CA, RS, and HQ, as shown in reactions Ox2b–Ox2c**. The PXR recombines with OH radicals to form PX2OH and PX4OH which, through acid/base catalyzed reactions, may tautomerize [68] to CA (Ox3b) and HQ (Ox3b*) respectively, as shown in reaction 3. Further reactions of CA and HQ with OH radicals (Ox3c and Ox3c*) yield 12QN and 14QN respectively, both of which have been identified experimentally [43, 46, 48, 69]. CA and HQ formed in other reactions may similarly be transformed into 12QN and 14QN. Reaction 4 shows how PXR may also react with H radicals to produce phenol (intermediates PX2H and PX4H are tautomerized to phenol).

PXR, PH2DHR, PH3DHR, and PH4DHR may also chain propagate with O_2 (path X.B in Fig. 1). For PXR, this reaction yields intermediate PX1O2, PX2O2 and PX4O2 radicals (reaction 5). Further reactions of PX2O2 with OH, H, and/or organic radicals yield 12QN. Reactions of PX4O2 with the same radicals result in the formation of 14QN. Because

Table 1 Calculated reaction Gibbs free energies, activation energies, and rate constants of reactions 1–5

Reaction	Reaction Gibbs free energy $\Delta_r G$ (kJ/mol)[a]	Activation energy E_a (kJ/mol)[a]	Rate constant (cm^3/molecule s)
PH + OH → PXR + H_2O (Reaction 1)	−139.0	4.8[b]	3.1×10^{-14}[b]
PH + OH → PH2DHR + H_2O (Reaction 2, Ox 2a)	−23.2	20.1	2.7×10^{-17}
PH + OH → PH3DHR + H_2O (Reaction 2, Ox2a*)	−29.1	17.1	1.3×10^{-15}
PH + OH → PH4DHR + H_2O (Reaction 2, Ox2a**)	−24.9	17.3	4.5×10^{-16}
PXR + OH → PX2OH (Reaction 3, Ox3a)	−201.1	No transition state	–
PX2OH → CA (Reaction 3, Ox3b)	−95.3	Overall reaction[c]	–
CA + 2OH → 12QN + $2H_2O$ (Reaction 3, Ox3c)	−370.7	Overall reaction[c]	–
PXR + OH → PX4OH (Reaction 3, Ox3a*)	−205.9	No transition state	–
PX4OH → HQ (Reaction 3, Ox3b*)	−91.2	Overall reaction[c]	–
HQ + 2OH → 14QN + $2H_2O$ (Reaction 3, Ox3c*)	−386.7	Overall reaction[c]	–
PXR + H→PX2H (Reaction 4, Ox4a)	−261.4	No transition state	–
PX2H → PH (Reaction 4, Ox4b)	−79.2	Overall reaction[c]	–
PXR + H→PH (Reaction 4, Ox4a*)	−340.6	No transition state	–
PXR + H→PX4H (Reaction 4, Ox4a**)	−270.1	No transition state	–
PX4H → PH (Reaction 4, Ox4b*)	−70.5	Overall reaction[c]	–
PXR + O_2 → PX1O2 (Reaction 5, Ox5a)	PX1O2 is not an energy minimum [78]	N/A	N/A
PXR + O_2 → PX2O2 (Reaction 5, Ox5a*)	50.3	55.2	9.9×10^{-25}
PXR + O_2 → PX4O2 (Reaction 5, Ox5a**)	36.5	54.7	8.8×10^{-24}

[a] Computed at PWPB95/ma-def2-TZVP//m062x/6-31+G(d,p) level

[b] Computed at m062x/6-311+G(2d,p)//m062x/midix level

[c] Multiple steps reaction

reaction 2 is not favorable (see the discussion that follows Table 1), further reactions of PH2DHR, PH3DHR, and PH4DHR radicals with O_2 were not considered.

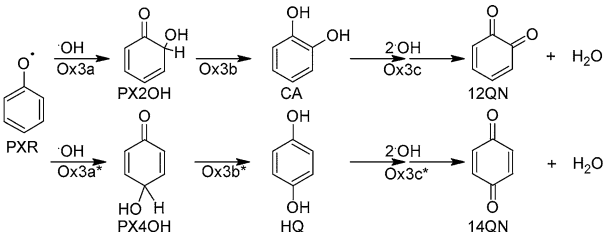

(3)

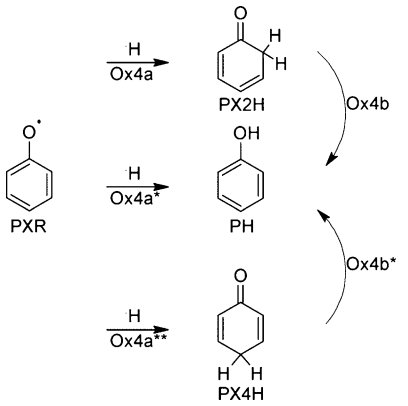

(4)

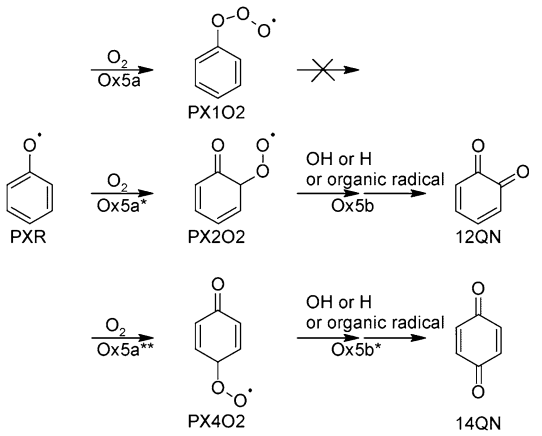

(5)

Table 1 shows calculated reaction Gibbs free energies, activation energies, and rate constants of reactions 1–5. Calculations performed at a low level of accuracy are shown in Table S1 in the supplementary material. A comparison of the Gibbs free energies of reactions 1 and 2 suggests that the phenolic H atom abstraction is more favorable than the phenol ring's H abstraction. Large differences in reaction Gibbs free energies between reactions 1 and 2 can be explained by resonance stabilization of phenoxyl radicals [70].

The transition states for reactions 1 and 2 were located successfully, which allowed for the calculation of the corresponding activation energies and reaction rate constants. As reported in Table 1, reaction 1 has an activation energy lower than any of the branches of reaction 2, indicating that the hydrogen abstraction most likely occurs on the OH group of the phenol ring. The calculated reaction rate constant for reaction 1 is 3.1×10^{-14} cm^3/molecule s, which is slightly lower than the experimentally determined value of 5×10^{-13} cm^3/molecule s [71]. Reaction rate constants computed for reactions Ox2a, Ox2a*, and Ox2a** are approximately two and three orders of magnitude lower than that of reaction 1. As a result, reactions Ox2a–Ox2a**, Ox2b–Ox2b**, and Ox2c–Ox2c** were excluded from further analysis. It is worth mentioning that the transition state search for reaction 1 at M062X/6-31+G(d,p)/IEF-PCM level failed. Instead, the activation energy for that reaction was computed at a lower calculation level (m062x/6-311+G(2d,p)//m062x/midix). As explained in the computational protocol, this may be due to the failure of the implicit solvation model.

The recombination reactions of PXR with OH radicals (reaction 3) to form tautomers PX2OH and PX4OH and finally 12QN and 14QN release large amounts of Gibbs free energy. Reactions of PXR with H radicals (reaction 4) are even more energetically favorable. However, because reactions Ox4a*, Ox4b, and Ox4b* yield phenol, they are difficult to verify experimentally. Radical recombination reactions, such as Ox3a, Ox3a*, Ox4a, Ox4a*, and Ox4a** do not have transition states; thus their rate constants cannot be computed by TST. Additionally, recombination reactions cannot be accurately described by the DFT method and their proper treatment requires sophisticated computation methods such as CASSCF [72]. The reactions Ox3b, Ox3b*, Ox4b, and Ox4b* are most likely acid/base catalyzed and do not have transition states either. It must be mentioned that a well-defined transition state for reaction Ox3b taking place in the gas phase does exist [10]. However, even though this gas phase reaction is catalyzed by a water molecule, in liquid phase the acid-catalyzed mechanism is probably faster [68].

Finally, the chain propagation reactions of the PXR radical with O_2 (reaction 5) are endergonic and are predicted to possess high activation energies. These calculations agree well with the ab initio calculations performed by McFerrin et al. [73] and Batiha et al. [12] as well as experimental measurements conducted by Hunter et al. [74] which confirmed that gas-phase chain propagation of PXR radical with O_2 is very slow. Given that the typical concentration of O_2 dissolved in water at 298 K and 1 bar is 7.6 mg/L [75] or 2.3×10^{-4} M and that the concentration of OH radicals produced by a gas discharge contacting water or direct liquid discharge ranges between $\sim 1.0 \times 10^{-13}$ and 1.0×10^{-10} M per 1 discharge pulse (calculation based on the reported rate of OH radical production at 30 kV [76, 77]), the reaction of O_2 with the PXR radical is still insignificant when compared with the rate of chain termination reaction of PXR with the OH radical, which was estimated to be on the order of $\sim 10^{-10}$ cm^3/molecule s [12]. However, for gas plasmas contacting water in an oxygen atmosphere where the concentration of O_2 near the interface could be 10 or 20 times that of OH radicals, the reaction between PXR and O_2 may become important. This gas phase reaction, however, cannot be compared to the results of this study which are valid only for reactions in liquids.

The most likely overall phenol oxidation reaction taking place via hydrogen abstraction is summarized in reaction 6, which is a combination of reactions 1 and 3. The formation of CA and HQ has been confirmed experimentally [26, 42, 43]. Both CA and HQ are further oxidized to 12QN and 14QN respectively.

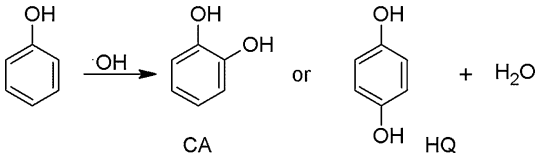

(6)

Path Y: OH Radical Addition to the Phenol Ring

To predict the site(s) of OH radical addition to phenol, a charge population analysis of phenol was performed. According to the hard soft acid base (HSAB) theory, the OH radical is a very hard electrophilic species [79], and the atomic charge population analysis of a substrate can accurately predict the relative likelihood of the site of OH radical attack. The natural population analysis charge (NPA charge), Hirschfield charge, and Merz–Singh–Kollman electron static potential fitting charge (MK charge) were calculated using Gaussian and Multiwfn software [80], and the results are shown in Table 2.

According to DeMatteo et al. [81], in the transition state of OH radical attack on an organic molecule, the OH radical abstracts a fraction of electron density from the organic substrate. In this state, the OH radical exhibits anionic nature while the organic substrate resembles a radical cation. Therefore, the OH radical has a strong preference to attack positions with high electron density, which can bring about a more stable radical cation transition state. The position with the lowest charge numerical value corresponds to the highest electron density hence is the preferred position of OH radical attack.

All three charge analysis methods predict that the *ortho* and *para* positions are the most reactive sites. The *ipso* position is least likely to be attacked and the reactivity of the *meta* position lies between these two extremes. Thus, the OH radical addition to the aromatic ring will result in the formation of three intermediates: PH2OHR, PH3OHR, and PH4OHR, as shown in reaction 7.

Reaction Gibbs free energies, activation energies, and rate constants for reactions Ox7–Ox7** are shown in Table 3. Calculations performed at a low level of accuracy are shown in Table S2 in the supplementary material. The results of both calculations indicate that

Table 2 Charge population analysis of phenol

Position of the carbon atom	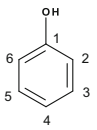		
	NPA charge	Hirschfield charge	MK charge
C1	0.324	0.069	0.433
C2	−0.293	−0.058	−0.282
C3	−0.190	−0.038	−0.092
C4	−0.244	−0.058	−0.214
C5	−0.188	−0.040	−0.050
C6	−0.261	−0.070	−0.382

additions to all three positions are possible and follow the sequence: *ortho* position (PH2OHR) > *para* position (PH4OHR) > *meta* position (PH3OHR). This agrees very well with the charge analysis results. It must be noted that the orientation of the hydroxyl group in phenol strongly influences the transition state geometry. Hence, OH radical addition to the *ortho* position on either side of the phenol molecule results in the formation of two qualitatively different structures. Due to the free rotation of the C–O bond, these two structures are essentially the same molecule; PH2OHR. For OH radical adding to the *meta* position, this interaction is weak and the difference between two *meta* positions can be ignored [10].

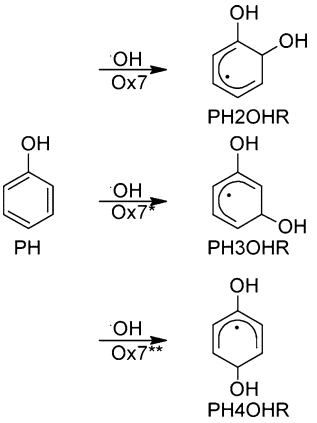

(7)

The rate constants calculated for the *ortho* (8.7×10^{-12} cm^3/molecule s) and *para* (4.7×10^{-12} cm^3/molecule s) position addition reactions are in excellent agreement with experimental findings (Table 3) even though the quality of this agreement is probably largely accidental.

It should be noted that the activation energy for the OH radical addition to the *ortho* and *para* position is negative. In fact, negative values of activation energy appear for some reactions reported later in Tables 5 and 7. This is due to the formation of tightly bound pre-

Table 3 Calculated reaction Gibbs free energies, activation energies, and rate constants of reaction 7

Reaction	Reaction Gibbs free energy $\Delta_r G$ (kJ/mol)	Activation energy E_a (kJ/mol)	Rate constant (cm^3/molecule s)	Experimental rate constant (cm^3/molecule s) at 298 K
PH + OH → PH2OHR[a] (Reaction 7, Ox 7)	−22.9	−6.3	5.1×10^{-12}	$(1.1–3.0) \times 10^{-11}$
PH + OH → PH2OHR[b] (Reaction 7, Ox 7)	−22.9	−5.5	3.6×10^{-12}	N/A
PH + OH → PH3OHR (Reaction 7, Ox 7*)	−24.0	5.4	1.9×10^{-12}	N/A
PH + OH → PH4OHR (Reaction 7, Ox 7**)	−31.5	−7.4	4.7×10^{-12}	N/A

[a] OH radical attack on the opposite side of the phenolic H atom

[b] OH radical attack on the same side as the phenolic H atom

reactive complexes which have significantly lower energy (around 20 kJ/mol according to our calculation performed at PWPB95/ma-def2-TZVPP//m062x/6-31+G(d,p) level) than the sum of individual energies of phenol and OH radical [10]. We purposely omitted the discussion on pre-reactive complexes because their geometries are complex and each TS may have several possible pre-reactive complexes. Determining the correct one (i.e., energy minimum) is time consuming and difficult. In addition, according to Bachrach [82], the reaction trajectories can skirt around the energy minima and directly form products.

In summary, the OH radical addition to the phenol ring most likely occurs on the *ortho* (PH2OHR) and *para* (PH4OHR) positions. However, because PH3OHR is a precursor to RS, an experimentally verified byproduct, subsequent reactions of this radical are also considered. Further reactions of PH2OHR, PH3OHR, and PH4OHR radicals involve recombination into stable products via any of the following four pathways: (Y.A) chain termination, (Y.B) chain propagation with O_2, (Y.C) radical elimination, and (Y.D) electron transfer. These individual pathways are discussed in subsequent sections.

Path Y.A: Chain Termination

Termination reactions of PH2OHR, PH3OHR, and PH4OHR radicals which include direct recombination with OH and H radicals form complex products. Because the unpaired electron in each of these radicals can be located on three different carbon atoms, each radical may form multiple stable products, as shown in Table 4. Reaction Gibbs free energy values confirm that all reaction products can be formed. Most of these products will undergo an acid–base catalyzed tautomerization reaction and transform into the corresponding ketone form. The formation of cyclohexa-1,5-diene-1,4-diol has been confirmed experimentally [42].

The recombination reactions between phenyl-derived organic radicals are another possibility, particularly when the initial phenol concentration is high. However, the recombination reactions of these radicals are extremely complex and dozens if not hundreds of reactions are equally likely to occur.

Path Y.B: Chain Propagation with O_2

PH2OHR, PH3OHR, and PH4OHR can further propagate with O_2 as shown in reaction 8, reaction 9, and reaction 10 respectively. To simplify the discussion, we only included the O_2 addition reactions to the opposite side as the added OH group (i.e., reactions of *trans* isomers). Tables 5, 6, and 7 show the calculated reaction Gibbs free energies, activation energies, and (reverse) rate constants for reaction 8, reaction 9, and reaction 10 respectively. Calculations performed at a low level of accuracy are shown in Table S3, Table S4, and Table S5 in the supplementary material. Reactions involving O_2 addition to the same side as the added OH group for only PH2OHR (i.e., reactions of *cis* isomers) are shown in the supplementary material as reaction S1. The calculated Gibbs free energies, activation energies, and (reverse) rate constants for the reaction S1 are reported in Table S6 in the supplementary material.

Because the unpaired electron is located only at the position *para* and *ortho* to the added OH group, reactions between the PH2OHR radical and O_2 will exclusively result in the formation of PH2OH1O2R, PH2OH3O2R, and PH2OH5O2R radicals (reaction 8). The fastest subsequent chain-propagation reactions of the PH2OH1O2R and PH2OH3O2R radicals yield CA. The PH2OH5O2R radical does not have further unimolecular reaction pathways. PH2OH1O2R may additionally undergo reaction Ox8f to generate muconic acid

Table 4 Possible products of termination reactions of PH2OHR, PH3OHR, and PH4OHR radicals

PH2OHR+OH	PH3OHR+OH	PH4OHR+OH
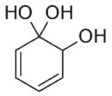 $\Delta_r G$=−253.1 kJ/mol cyclohexa-3,5-diene-1,1,2-triol	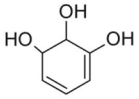 $\Delta_r G$=−243.2 kJ/mol cyclohexa-3,5-diene-1,2,3-triol	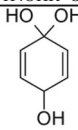 $\Delta_r G$=−253.9 kJ/mol cyclohexa-2,5-diene-1,1,4-triol
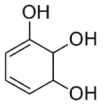 $\Delta_r G$=−249.4 kJ/mol cyclohexa-3,5-diene-1,2,3-triol	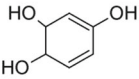 $\Delta_r G$=−249.0 kJ/mol cyclohexa-3,5-diene-1,2,4-triol	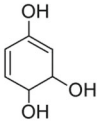 $\Delta_r G$=−244.4 kJ/mol cyclohexa-3,5-diene-1,2,4-triol
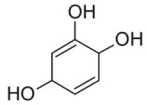 $\Delta_r G$=−240.2 kJ/mol cyclohexa-2,5-diene-1,2,4-triol	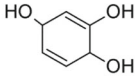 $\Delta_r G$=−211.6 kJ/mol cyclohexa-2,5-diene-1,2,4-triol	
PH2OHR+H	**PH3OHR+H**	**PH4OHR+H**
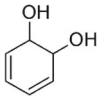 $\Delta_r G$=−273.7 kJ/mol cyclohexa-3,5-diene-1,2-diol	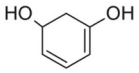 $\Delta_r G$=−296.8 kJ/mol cyclohexa-3,5-diene-1,3-diol	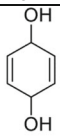 $\Delta_r G$=−271.3 kJ/mol cyclohexa-2,5-diene-1,4-diol
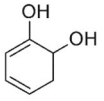 $\Delta_r G$=−295.4 kJ/mol cyclohexa-2,4-diene-1,2-diol	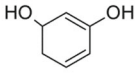 $\Delta_r G$=−303.1 kJ/mol cyclohexa-1,5-diene-1,3-diol	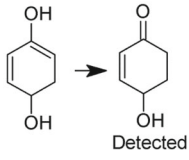 Detected $\Delta_r G$=−284.5 kJ/mol cyclohexa-1,5-diene-1,4-diol
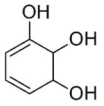 $\Delta_r G$=−291.8 kJ/mol cyclohexa-2,5-diene-1,2-diol		

[83] and Ox8d to generate an unsaturated organic acid containing an epoxy functional group (PO4) [24]. Although reactions Ox8f–Ox8h release large amounts of free energy, reaction Ox8f is significantly slower than Ox8b indicating that muconic acid will not be formed via this pathway (Table 5). The "epoxy pathway", which is based on atmospheric chemistry findings [23], is extremely complicated as it involves a large amount of branching and hundreds of possible intermediate structures, in addition to simple cyclization steps assumed to follow reaction Ox8d. Compared to reaction Ox8b, the

Table 5 Calculated reaction Gibbs free energies, activation energies, and rate constants of reaction 8

Reaction	Reaction Gibbs free energy $\Delta_r G$ (kJ/mol)	Activation energy E_a (kJ/mol)	Rate constant	Reverse rate constant
PH2OHR + O_2 ⇌ PH2OH1O2R (Reaction 8, Ox8a)	−2.4	3.7	1.6×10^{-15a}	1.5×10^{4b}
PH2OH1O2R → CA + HO_2 (Reaction 8, Ox8b)	−153.3	37.0	1.2×10^{6b}	–
PH2OH1O2R → PX2OH + HO_2 (Reaction 8, Ox8b*)	−55.7	31.0	3.9×10^{7b}	–
PX2OH → CA (Reaction 8, Ox8c)	−95.3	Overall reaction[c]	–	–
PH2OH1O2R → PO3 (Reaction 8, Ox8d)	−24.5	57.4	1.0×10^{2b}	–
PO3 + OH → PO4 + H_2O (Reaction 8, Ox8e)	−560.0	Overall reaction[c]	–	–
PH2OH1O2R → CA1OOH (Reaction 8, Ox8f)	−63.3	84.4	7.9×10^{-3b}	–
CA1OOH → PHW1 (Reaction 8, Ox8g)	−192.1	79.2	3.7×10^{-1b}	–
PHW1 + OH → Muconic acid + H_2O (Reaction 8, Ox8h)	−324.3	Overall reaction[c]	N/A	–
PH2OHR + O_2 ⇌ PH2OH3O2R (Reaction 8, Ox8a*)	−0.6	2.1	2.4×10^{-15a}	7.3×10^{4b}
PH2OH3O2R → CA + HO_2 (Reaction 8, Ox8b**)	−153.3	41.2	3.0×10^{5b}	–
PH2OHR + O_2 ⇌ PH2OH5O2R (Reaction 8, Ox8a**)	−5.1	−6.3	2.2×10^{-14a}	6.9×10^{4b}

[a] cm^3/molecule s

[b] 1/s

[c] Multiple steps reaction

formation of PO3 requires high activation energy making the epoxy pathway not feasible (Table 5).

Reaction rate constants calculated in Table 5 reveal that reactions Ox8b and Ox8b** are significantly slower compared to Ox8b*. This is because the strong hydrogen bond between the O_2 functional group and the alpha-OH functional group in PH2OH1O2R* significantly stabilizes the transition state structure. PX2OH formed in reaction Ox8b* is immediately converted to CA and is the main intermediate in the production of CA from PH2OHR. Reaction Ox8b* is well-known and frequently occurs in atmospheric chemistry [10, 22].

Reactions of PH3OHR with O_2 yield RS, as shown in reaction 9. The intermediate PH3OH6O2R formed in reaction Ox9a** does not have further reaction pathways. According to the values reported in Table 6, RS will most likely be formed in reactions Ox9a and Ox9b. HQ is formed in reaction of PH4OHR radical with O_2 (reaction 10). Reaction rate constants reported in Table 7 reveal that this molecule will most likely be

Table 6 Calculated reaction Gibbs free energies, activation energies, and rate constants of reaction 9

Reaction	Reaction Gibbs free energy $\Delta_r G$ (kJ/mol)	Activation energy E_a (kJ/mol)	Rate constant	Reverse rate constant
PH3OHR + O_2 ⇌ PH3OH2O2R (Reaction 9, Ox9a)	−3.1	20.9	1.3×10^{-18}[a]	9.3[b]
PH3OH2O2R → RS + HO_2 (Reaction 9, Ox9b)	−163.4	53.1	2.0×10^{3}[b]	–
PH3OHR + O_2 ⇌ PH3OH4O2R (Reaction 9, Ox9a*)	−8.7	21.2	1.3×10^{-18}[a]	1.0[b]
PH3OH4O2R → RS + HO_2 (Reaction 9, Ox9b*)	−157.9	60.2	1.4×10^{2}[b]	–
PH3OHR + O_2 ⇌ PH3OH6O2R (Reaction 9, Ox9a**)	7.3	8.5	9.9×10^{-17}[a]	4.7×10^{2}[b]

[a] cm^3/molecule s

[b] 1/s

Table 7 Calculated reaction Gibbs free energies, activation energies, and rate constants of reaction 10

Reaction	Reaction free energy $\Delta_r G$ (kJ/mol)	Activation energy E_a (kJ/mol)	Rate constant	Reverse rate constant
PH4OHR + O_2 ⇌ PH4OH1O2R (Reaction 10, Ox10a)	0.0	−16.8	8.4×10^{-13}[a]	1.8×10^{7}[b]
PH4OH1O2R → PX4OH + HO_2 (Reaction 10, Ox10b)	−63.3	19.6	8.2×10^{9}[b]	–
PX4OH → HQ (Reaction 10, Ox10c)	−91.2	Overall reaction[c]	–	–
PH4OHR + O_2 ⇌ PH4OH3O2R (Reaction 10, Ox10a*)	−10.2	1.6	2.2×10^{-15}[a]	8.8×10^{2}[b]
PH4OH3O2R → HQ + HO_2 (Reaction 10, Ox10b*)	−144.8	44.7	6.9×10^{4}[b]	–

[a] cm^3/molecule s

[b] 1/s

[c] Multiple steps reaction

formed from the PH4OH3O2R intermediate. For the O_2 adducts PH2OH5O2R and PH3OH6O2R that do not have further reaction pathways, the reverse reaction that converts the adduct back to PH2OHR or PH3OHR is the most likely path.

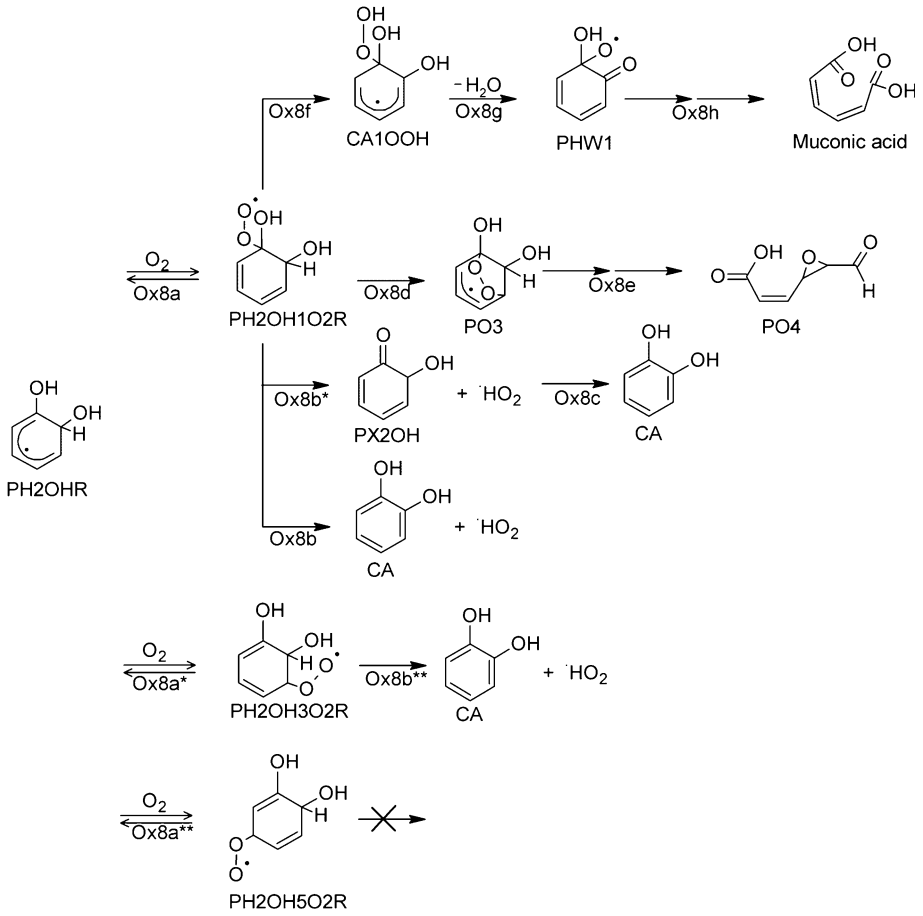
Ox8f
CA1OOH
$-H_2O$
Ox8g
PHW1
Ox8h
Muconic acid
O_2
Ox8a
PH2OH1O2R
Ox8d
PO3
Ox8e
PO4
PH2OHR
Ox8b*
PX2OH
+ HO_2
Ox8c
CA
Ox8b
CA
+ HO_2
O_2
Ox8a*
PH2OH3O2R
Ox8b**
CA
+ HO_2
O_2
Ox8a**
PH2OH5O2R

(8)

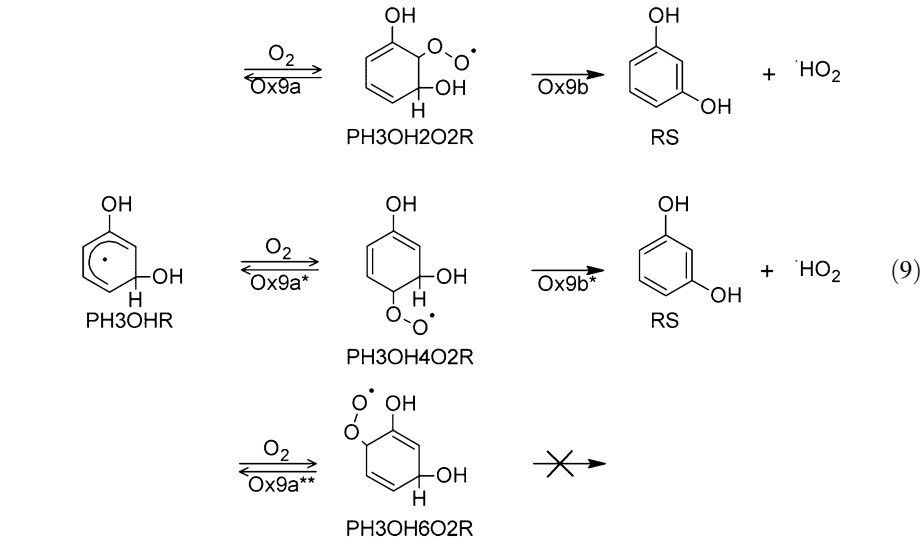

(9)

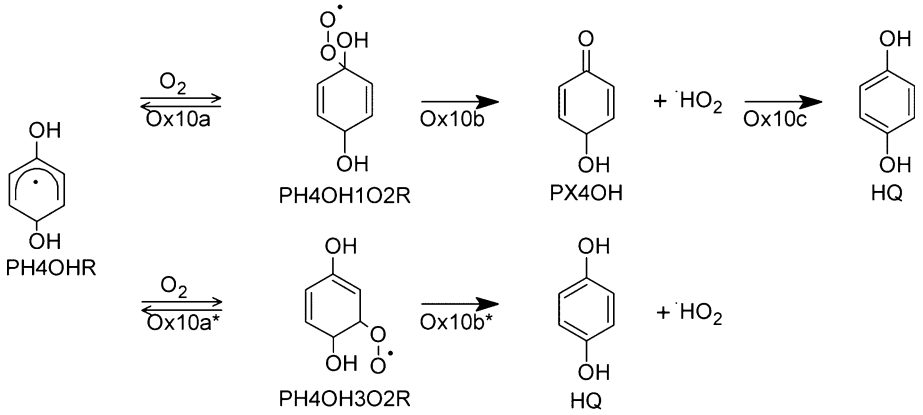

(10)

To summarize, OH radical addition to phenol most likely generates PH2OHR and PH4OHR radicals which can chain propagate with O_2 to yield CA and HQ respectively, as shown in reaction 11. Because PH3OHR radicals are formed in very low concentrations, chain propagation with O_2 will not yield significant concentrations of RS.

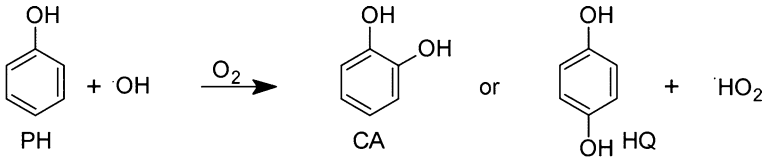

(11)

Path Y.C: Radical Elimination

The chain propagation of PH2OHR, PH3OHR, and PH4OHR radicals via radical elimination assumes the loss of an H atom and/or OH group, as shown in reactions 12 and 13 respectively. According to the values reported in Table 8, reaction 12 is not possible. Reactions Ox12, Ox12*, and Ox12** are predicted to possess extremely high activation energies and thus very low reaction rates. Reaction 13 is predicted to be possible but occurs at very low rates and results in the formation of phenol. Therefore, radical elimination was disqualified as a contributing mechanism to the phenol degradation pathway. Table 7 shows the calculated reaction Gibbs free energies, activation energies, and rate constants for reactions 12 and 13. Calculations performed at a low level of accuracy are shown in Table S7 in the supplementary material.

Table 8 Calculated Gibbs free energies, activation energies, and rate constants of reactions 12 and 13

Reaction	Reaction Gibbs free energy $\Delta_r G$ (kJ/mol)	Activation energy E_a (kJ/mol)	Rate constant (1/s)
PH2OHR → CA + H (Reaction 12, Ox12)	47.8	107.3	1.3×10^{-6}
PH3OHR → RS + H (Reaction 12, Ox12*)	66.5	99.9	1.3×10^{-5}
PH4OHR → HQ + H (Reaction 12, Ox12**)	55.6	107.2	7.1×10^{-7}
PH2OHR → PH + OH (Reaction 13, Ox13)	20.9	57.6	1.5×10^{3}
PH3OHR → PH + OH (Reaction 13, Ox13*)	14.3	57.5	2.7×10^{3}
PH4OHR → PH + OH (Reaction 13, Ox13**)	19.7	50.0	2.6×10^{4}

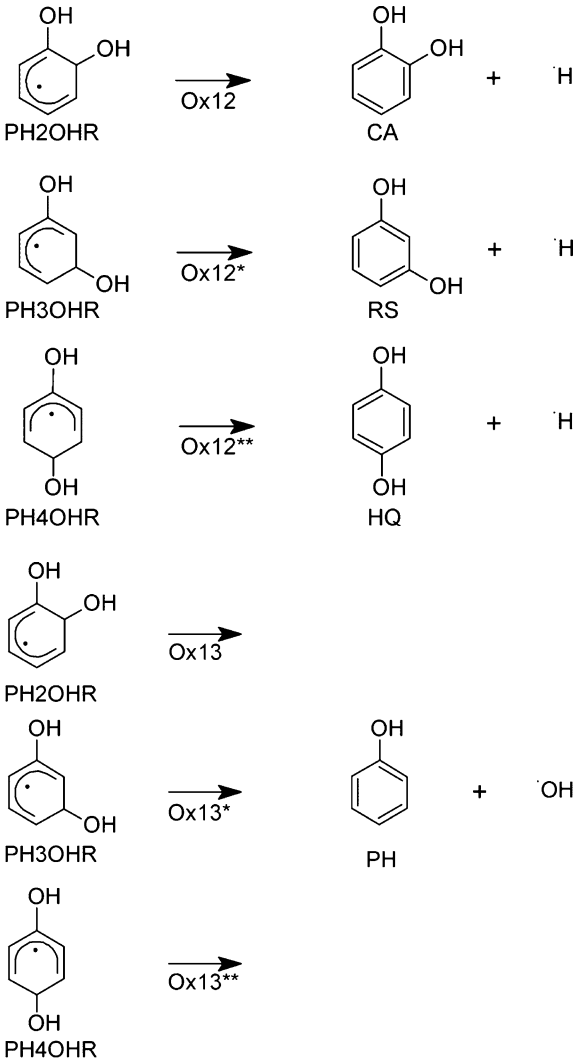

(12)

(13)

Path Y.D: Electron Transfer

Electron transfer is a somewhat different reaction channel that can rapidly convert PH2OHR, PH3OHR, and PH4OHR radicals into stable products (reaction 14). Standard electrode potentials for the half reactions of these three intermediates are listed in Table 9. The same table reports the oxidation potentials of OH and HO_2 radicals, H_2O_2 and O_2, the most common plasma oxidants.

Table 9 Electrode potentials of redox pairs shown in reaction 14 and selected oxygenated species

Reaction	Electrode potential (V)	
	Calculated	Literature
PH2OHR/PH2OHC	−0.15	N/A
PH3OHR/PH3OHC	0.29	N/A
PH4OHR/PH4OHC	−0.28	N/A
OH/H_2O	2.80	2.81 [84]
HO_2/H_2O_2	1.35	1.06 [85]
H_2O_2/H_2O	1.93	1.76 [84]
O_2/H_2O	1.30	1.23 [86]

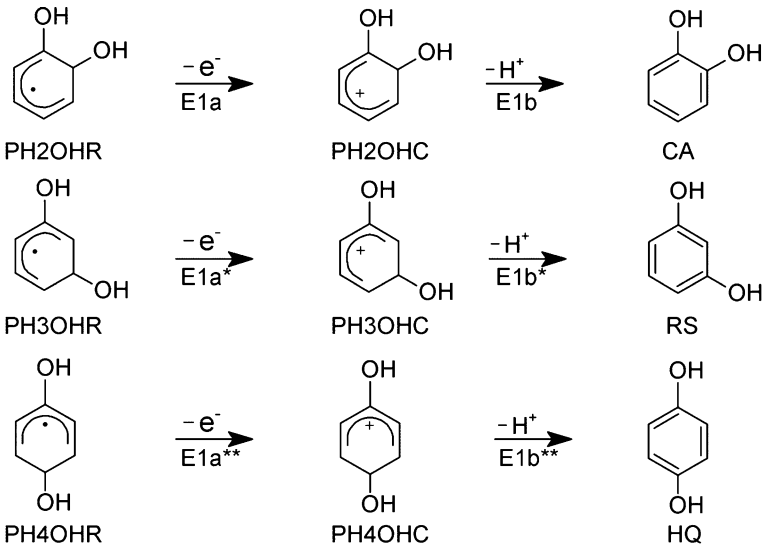

(14)

Half reactions of PH2OHR and PH4OHR and, to some extent, PH3OHR radicals are characterized by negative reduction potentials, indicating the strong reduction ability of these organic radicals. Through intermediate compounds such as benzoquinone or transition metal complexes that serve as an electron transfer shuttle, OH radicals as well as H_2O_2, HO_2 and O_2, which might exist in relatively large concentrations, can easily oxidize PH2OHR, PH3OHR, and PH4OHR radicals into corresponding cations (reactions E1a, E1a*, and E1a**), which then immediately dissociate into CA, RS, and HQ respectively. Because the structures of PH2OHC, PH3OHC, and PH4OHC intermediates are very similar to those of PH2OHR, PH3OHR, and PH4OHR radicals, the reorganization energy involved in forming these byproducts is very small leading to high reaction rates [87]. Thus, electron transfer reactions of PH2OHR, PH3OHR, and PH4OHR radicals are highly probable pathways for the production of CA, RS, and HQ respectively. The importance of electron transfer reactions has been confirmed experimentally [88].

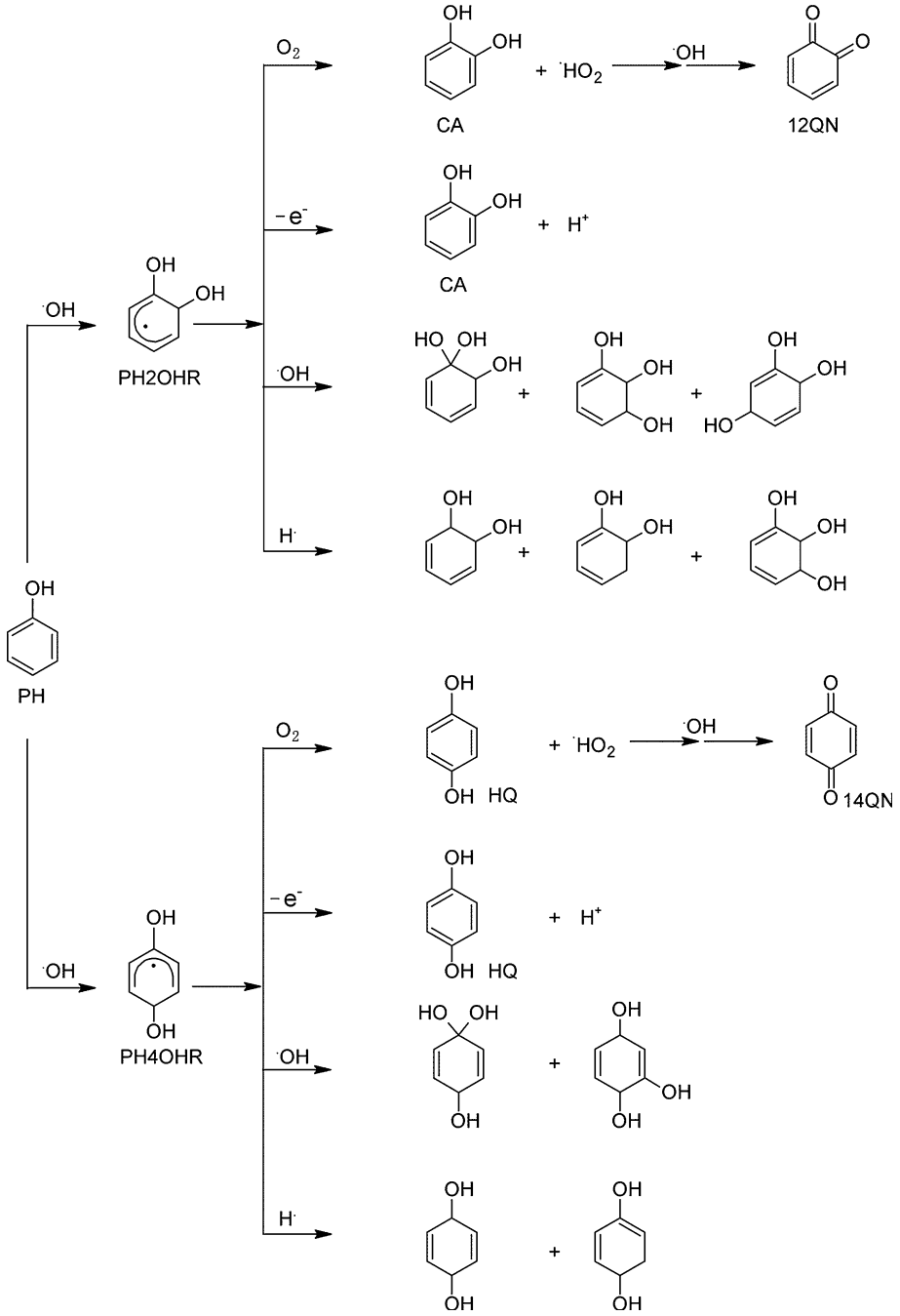

Scheme 1 The most likely reaction pathways phenol undergoes upon OH radical attack

Conclusions

The study used DFT simulations to investigate the most probable reaction pathways of OH radical electrophilic attack on phenol. OH radicals react with phenol via two general pathways; they either abstract an H atom from the phenol ring or they add to the ring. The calculated activation energies and reaction rate constants indicate that phenolic H abstraction is less likely to occur than OH addition, which will be the fastest in the *ortho* and *para* positions. The chain propagation with molecular oxygen of such formed *ortho* and *para* dihydroxycyclohexadienyl radicals will result in the production of hydroquinone and catechol, which are, concurrently, the most likely products of phenol degradation by OH radicals. The reaction of *meta* dihydroxycyclohexadienyl radicals with oxygen may also yield small concentrations of resorcinol.

Catechol, resorcinol, and hydroquinone may also be formed in electron transfer reactions of *ortho, meta,* and *para* dihydroxycyclohexadienyl radicals with OH radicals, HO_2 radicals, O_2, and/or H_2O_2 respectively. In the absence of high concentrations of molecular oxygen, these electron transfer reactions might also be the only reaction pathway for the production of RS. Scheme 1 summarizes the most likely phenol hydroxylation reactions.

With the exception of the dienes, all the stable products predicted by the model have been verified experimentally. Two important findings of this study are: (1) the rate of abstraction of the H atoms from the phenol ring by OH radicals is slow, and (2) electron transfer is an important reaction channel for forming stable products. Future modelers may wish to consider these findings. In conclusion, the results of this study are broadly applicable to other oxidation technologies that involve reactions of OH radicals with organic compounds.

Acknowledgements One of the authors (S. Mededovic Thagard) would like to acknowledge the support of the National Science Foundation (CBET: #1336385).

References

1. Buxton GV, Greenstock CL, Helman WP, Ross AB (1988) Critical review of rate constants for reactions of hydrated electrons, hydrogen atoms and hydroxyl radicals $^{\cdot}OH/^{\cdot}O^{-}$ in aqueous solution. J Phys Chem Ref Data 17(2):513–886
2. Bielski B, Arudi RL, Sutherland MW (1983) A study of the reactivity of HO_2/O_2^{-} with unsaturated fatty acids. J Biol Chem 258(8):4759–4761
3. Ren X, Sun Y, Fu X, Zhu L, Cui Z (2013) DFT comparison of the OH-initiated degradation mechanisms for five chlorophenoxy herbicides. J Mol Model 19(6):2249–2263
4. Niu J, Lin H, Gong C, Sun X (2013) Theoretical and experimental insights into the electrochemical mineralization mechanism of perfluorooctanoic acid. Environ Sci Technol 47(24):14341–14349
5. Zhang C, Sun T, Sun X (2011) Mechanism for OH-initiated degradation of 2,3,7,8-tetrachlorinated dibenzo-*p*-dioxins in the presence of O_2 and NO/H_2O. Environ Sci Technol 45(11):4756–4762
6. Manoj P, Prasanthkumar K, Manoj V, Aravind UK, Manojkumar T, Aravindakumar C (2007) Oxidation of substituted triazines by sulfate radical anion ($SO_4^{\cdot} -$) in aqueous medium: a laser flash photolysis and steady state radiolysis study. J Phys Org Chem 20(2):122–129
7. Wang Y, Liu Y, Luo Y, Zhang W, Zhong R (2006) Theoretical study on the mechanisms of the reaction of peroxynitrous acid and phenol. Acta Phys Chem Sin 22(10):1266–1272
8. Ramos B, Farah J, Teixeira A (2012) Estimating reaction constants by ab initio molecular modeling: a study on the oxidation of phenol to catechol and hydroquinone in advanced oxidation processes. Braz J Chem Eng 29(1):113–120
9. Jayathilaka PB, Pathiraja GC, Bandara A, Subasinghe ND, Nanayakkara N (2014) Theoretical study of phenol and hydroxyl radical reaction mechanism in aqueous medium by the DFT/B3LYP/6-31 + G (d, p)/CPCM model. Can J Chem 92(9):809–813

10. Xu C, Wang L (2013) Atmospheric oxidation mechanism of phenol initiated by OH radical. J Phys Chem A 117(11):2358–2364
11. Carrier M, Guillard C, Besson M, Bordes C, Chermette H (2009) Photocatalytic degradation of diuron: experimental analyses and simulation of HO radical attacks by density functional theory calculations. J Phys Chem A 113(22):6365–6374
12. Batiha M, Al-Muhtaseb AAH, Altarawneh M (2012) Theoretical study on the reaction of the phenoxy radical with O_2, OH, and NO_2. Int J Quantum Chem 112(3):848–857
13. Huang Y, Huang Y, Tsai H, Chen H (2010) Degradation of phenol using low concentration of ferric ions by the photo-Fenton process. J Taiwan Inst Chem Eng 41(6):699–704
14. Bossmann SH, Oliveros E, Göb S, Siegwart S, Dahlen EP, Payawan L, Straub M, Wörner M, Braun AM (1998) New evidence against hydroxyl radicals as reactive intermediates in the thermal and photochemically enhanced Fenton reactions. J Phys Chem A 102(28):5542–5550
15. Bremner DH, Burgess AE, Houllemare D, Namkung K-C (2006) Phenol degradation using hydroxyl radicals generated from zero-valent iron and hydrogen peroxide. Appl Catal B 63(1):15–19
16. Zazo J, Casas J, Mohedano A, Gilarranz M, Rodriguez J (2005) Chemical pathway and kinetics of phenol oxidation by Fenton's reagent. Environ Sci Technol 39(23):9295–9302
17. Kwon BG, Lee DS, Kang N, Yoon J (1999) Characteristics of *p*-chlorophenol oxidation by Fenton's reagent. Water Res 33(9):2110–2118
18. Mijangos F, Varona F, Villota N (2006) Changes in solution color during phenol oxidation by Fenton reagent. Environ Sci Technol 40(17):5538–5543
19. Feng J, Hu X, Yue PL (2004) Degradation of salicylic acid by photo-assisted Fenton reaction using Fe ions on strongly acidic ion exchange resin as catalyst. Chem Eng J 100(1):159–165
20. Grymonpré DR, Sharma AK, Finney WC, Locke BR (2001) The role of Fenton's reaction in aqueous phase pulsed streamer corona reactors. Chem Eng J 82(1):189–207
21. Bloss C, Wagner V, Jenkin M, Volkamer R, Bloss W, Lee J, Heard D, Wirtz K, Martin-Reviejo M, Rea G (2005) Development of a detailed chemical mechanism (MCMv3. 1) for the atmospheric oxidation of aromatic hydrocarbons. Atmos Chem Phys 5(3):641–664
22. Atkinson R, Arey J (2003) Atmospheric degradation of volatile organic compounds. Chem Rev 103(12):4605–4638
23. Atkinson R, Carter WP, Darnall KR, Winer AM, Pitts JN (1980) A smog chamber and modeling study of the gas phase NO_x–air photooxidation of toluene and the cresols. Int J Chem Kinet 12(11):779–836
24. Jenkin M, Saunders S, Wagner V, Pilling M (2003) Protocol for the development of the master chemical mechanism, MCM v3 (part B): tropospheric degradation of aromatic volatile organic compounds. Atmos Chem Phys 3(1):181–193
25. Wagner V, Jenkin M, Saunders S, Stanton J, Wirtz K, Pilling M (2003) Modelling of the photooxidation of toluene: conceptual ideas for validating detailed mechanisms. Atmos Chem Phys 3(1):89–106
26. Wang H, Li J, Quan X, Wu Y, Li G, Wang F (2007) Formation of hydrogen peroxide and degradation of phenol in synergistic system of pulsed corona discharge combined with TiO_2 photocatalysis. J Hazard Mater 141(1):336–343
27. Ding Z, Lu G, Greenfield P (2000) Role of the crystallite phase of TiO_2 in heterogeneous photocatalysis for phenol oxidation in water. J Phys Chem. B 104(19):4815–4820
28. Serpone N, Maruthamuthu P, Pichat P, Pelizzetti E, Hidaka H (1995) Exploiting the interparticle electron transfer process in the photocatalysed oxidation of phenol, 2-chlorophenol and pentachlorophenol: chemical evidence for electron and hole transfer between coupled semiconductors. J Photochem Photobiol, A 85(3):247–255
29. Doong R, Chen C, Maithreepala R, Chang S (2001) The influence of pH and cadmium sulfide on the photocatalytic degradation of 2-chlorophenol in titanium dioxide suspensions. Water Res 35(12):2873–2880
30. Scheck CK, Frimmel FH (1995) Degradation of phenol and salicylic acid by ultraviolet radiation/hydrogen peroxide/oxygen. Water Res 29(10):2346–2352
31. Chitose N, Ueta S, Seino S, Yamamoto TA (2003) Radiolysis of aqueous phenol solutions with nanoparticles. 1. Phenol degradation and TOC removal in solutions containing TiO_2 induced by UV, γ-ray and electron beams. Chemosphere 50(8):1007–1013
32. Nageswara Rao A, Sivasankar B, Sadasivam V (2009) Kinetic study on the photocatalytic degradation of salicylic acid using ZnO catalyst. J Hazard Mater 166(2):1357–1361
33. Kubesch K, Zona R, Solar S, Gehringer P (2005) Degradation of catechol by ionizing radiation, ozone and the combined process ozone-electron-beam. Radiat Phys Chem 72(4):447–453
34. Duarte C, Sampa M, Rela P, Oikawa H, Silveira C, Azevedo A (2002) Advanced oxidation process by electron-beam-irradiation-induced decomposition of pollutants in industrial effluents. Radiat Phys Chem 63(3):647–651

35. Lin K, Cooper WJ, Nickelsen MG, Kurucz CN, Waite TD (1995) Decomposition of aqueous solutions of phenol using high energy electron beam irradiation—a large scale study. Appl Radiat Isot 46(12):1307–1316
36. Li X, Cui Y, Feng Y, Xie Z, Gu J (2005) Reaction pathways and mechanisms of the electrochemical degradation of phenol on different electrodes. Water Res 39(10):1972–1981
37. Papouchado L, Sandford R, Petrie G, Adams R (1975) Anodic oxidation pathways of phenolic compounds Part 2. Stepwise electron transfers and coupled hydroxylations. J Electroanal Chem Interfacial Electrochem 65(1):275–284
38. Comninellis C, Nerini A (1995) Anodic oxidation of phenol in the presence of NaCl for wastewater treatment. J Appl Electrochem 25(1):23–28
39. Comninellis C, Pulgarin C (1991) Anodic oxidation of phenol for waste water treatment. J Appl Electrochem 21(8):703–708
40. Tezuka M, Iwasaki M (1998) Plasma induced degradation of chlorophenols in an aqueous solution. Thin Solid Films 316(1):123–127
41. Yuan M, Watanabe T, Chang C (2010) DC water plasma at atmospheric pressure for the treatment of aqueous phenol. Environ Sci Technol 44(12):4710–4715
42. Satoh K, Murakami M, Itoh H (2013) Pulsed-plasma degradation of phenol in an aqueous solution. In: 21st international symposium on plasma chemistry (ISPC 21), Cairns Convention Centre, Queensland, Australia
43. Liu Y, Jiang X (2005) Phenol degradation by a nonpulsed diaphragm glow discharge in an aqueous solution. Environ Sci Technol 39(21):8512–8517
44. Hoeben W, Van Veldhuizen E, Rutgers W, Cramers C, Kroesen G (2000) The degradation of aqueous phenol solutions by pulsed positive corona discharges. Plasma Sources Sci Technol 9(3):361
45. Hoeben W, Van Veldhuizen E, Rutgers W, Kroesen G (1999) Gas phase corona discharges for oxidation of phenol in an aqueous solution. J Phys D Appl Phys 32(24):L133
46. Hoeben WFLM (2000) Pulsed corona-induced degradation of organic materials in water. Ph.D. Dissertation, Technische Universiteit Eindhoven, Eindhoven
47. Lukes P, Locke BR (2005) Degradation of substituted phenols in a hybrid gas-liquid electrical discharge reactor. Ind Eng Chem Res 44(9):2921–2930
48. Lukes P (2001) Water treatment by pulsed streamer corona discharge. Ph.D. Thesis, Prague
49. Li J, Sato M, Ohshima T (2007) Degradation of phenol in water using a gas–liquid phase pulsed discharge plasma reactor. Thin Solid Films 515(9):4283–4288
50. Hayashi D, Hoeben W, Dooms G, Van Veldhuizen E, Rutgers W, Kroesen G (2000) Influence of gaseous atmosphere on corona-induced degradation of aqueous phenol. J Phys D Appl Phys 33(21):2769
51. Sano N, Kawashima T, Fujikawa J, Fujimoto T, Kitai T, Kanki T, Toyoda A (2002) Decomposition of organic compounds in water by direct contact of gas corona discharge: influence of discharge conditions. Ind Eng Chem Res 41(24):5906–5911
52. Sharma A, Locke B, Arce P, Finney W (1993) A preliminary study of pulsed streamer corona discharge for the degradation of phenol in aqueous solutions. Hazard Waste Hazard Mater 10(2):209–219
53. Sugiarto AT, Sato M (2001) Pulsed plasma processing of organic compounds in aqueous solution. Thin Solid Films 386(2):295–299
54. Tothova I, Lukes P, Clupek M, Babicky V, Janda V (2009) Removal of nonylphenol by pulsed corona discharge in water. In: 19th international symposium on plasma chemistry, Bochum
55. Scuseria G, Robb M, Cheeseman J, Scalmani G, Barone V, Mennucci B, Petersson G, Nakatsuji H, Caricato M, Li X (2009) Gaussian 09, Revision D. 01. Gaussian Inc., Wallingford, CT
56. Ditchfield R, Hehre W, Pople JA (1971) Self-consistent molecular-orbital methods. 9. extended gaussian-type basis for molecular-orbital studies of organic molecules. J Chem Phys 54(2):724–728
57. Zhao Y, Truhlar DG (2008) The M06 suite of density functionals for main group thermochemistry, thermochemical kinetics, noncovalent interactions, excited states, and transition elements: two new functionals and systematic testing of four M06-class functionals and 12 other functionals. Theor Chem Acc 120(1–3):215–241
58. Tomasi J, Mennucci B, Cances E (1999) The IEF version of the PCM solvation method: an overview of a new method addressed to study molecular solutes at the QM ab initio level. J Mol Struct 464(1):211–226
59. Neese F (2012) The ORCA program system. WIREs Comput Mol Sci 2(1):73–78
60. Goerigk L, Grimme S (2011) A thorough benchmark of density functional methods for general main group thermochemistry, kinetics, and noncovalent interactions. PCCP 13(14):6670–6688
61. Weigend F, Ahlrichs R (2005) Balanced basis sets of split valence, triple zeta valence and quadruple zeta valence quality for H to Rn: design and assessment of accuracy. PCCP 7(18):3297–3305

62. Marenich AV, Cramer CJ, Truhlar DG (2009) Universal solvation model based on solute electron density and on a continuum model of the solvent defined by the bulk dielectric constant and atomic surface tensions. J Phys Chem B 113(18):6378–6396
63. Goerigk L, Grimme S (2010) Efficient and accurate double-hybrid-meta-GGA density functionals· evaluation with the extended GMTKN30 database for general main group thermochemistry, kinetics, and noncovalent interactions. J Chem Theory Comput 7(2):291–309
64. Marenich AV, Ho J, Coote ML, Cramer CJ, Truhlar DG (2014) Computational electrochemistry: prediction of liquid-phase reduction potentials. PCCP 16(29):15068–15106
65. Li X, Frisch MJ (2006) Energy-represented direct inversion in the iterative subspace within a hybrid geometry optimization method. J Chem Theory Comput 2(3):835–839
66. Peng C, Bernhard Schlegel H (1993) Combining synchronous transit and quasi-newton methods to find transition states. Isr J Chem 33(4):449–454
67. Wigner EP (1997) Über das Überschreiten von Potentialschwellen bei chemischen Reaktionen. In: Wightman A (ed) Part I: physical chemistry. Part II: solid state physics, vol 4. Springer, Berlin, pp 96–109
68. Wirz J (2010) Kinetic studies of keto-enol and other tautomeric equilibria by flash photolysis. Adv Phys Org Chem 44:325
69. Gao J, Liu Y, Yang W, Pu L, Yu J, Lu Q (2003) Oxidative degradation of phenol in aqueous electrolyte induced by plasma from a direct glow discharge. Plasma Sources Sci Technol 12(4):533
70. Bordwell FG, Cheng J (1991) Substituent effects on the stabilities of phenoxyl radicals and the acidities of phenoxyl radical cations. J Am Chem Soc 113(5):1736–1743
71. Knispel R, Koch R, Siese M, Zetzsch C (1990) Adduct formation of OH radicals with benzene, toluene, and phenol and consecutive reactions of the adducts with NO_x and O_2. Ber Bunsenges Phys Chem 94(11):1375–1379
72. Sherrill CD (2005) Chapter 4: Bond breaking in quantum chemistry. In: Annual reports in computational chemistry, vol 1. Elsevier, Amsterdam, pp 45–56
73. McFerrin CA, Hall RW, Dellinger B (2008) *Ab initio* study of the formation and degradation reactions of semiquinone and phenoxyl radicals. J Mol Struct 848(1):16–23
74. Hunter EP, Desrosiers MF, Simic MG (1989) The effect of oxygen, antioxidants, and superoxide radical on tyrosine phenoxyl radical dimerization. Free Radic Biol Med 6(6):581–585
75. Weiss R (1970) The solubility of nitrogen, oxygen and argon in water and seawater. Deep-Sea Res Oceanogr Abstr 17:721–735
76. Kanazawa S, Kawano H, Watanabe S, Furuki T, Akamine S, Ichiki R, Ohkubo T, Kocik M, Mizeraczyk J (2011) Observation of OH radicals produced by pulsed discharges on the surface of a liquid. Plasma Sources Sci Technol 20(3):034010
77. Sahni M (2006) Analysis of the chemical reactions in pulsed streamer discharges: an experimental study. Ph.D. Dissertation, Florida State University, Tallahassee
78. Hu H, Dibble TS (2013) Quantum chemistry, reaction kinetics, and tunneling effects in the reaction of methoxy radicals with O_2. J Phys Chem A 117(51):14230–14242
79. Nguyen HMT, Peeters J, Nguyen MT, Chandra AK (2004) Use of DFT-based reactivity descriptors for rationalizing radical reactions: a critical analysis. J Phys Chem A 108(3):484–489
80. Lu T, Chen F (2012) Multiwfn: a multifunctional wavefunction analyzer. J Comput Chem 33(5):580–592
81. DeMatteo MP, Poole JS, Shi X, Sachdeva R, Hatcher PG, Hadad CM, Platz MS (2005) On the electrophilicity of hydroxyl radical: a laser flash photolysis and computational study. J Am Chem Soc 127(19):7094–7109
82. Bachrach SM (2014) Computational organic chemistry. Wiley, New York
83. Sawaki Y, Foote CS (1983) Mechanism of carbon-carbon cleavage of cyclic 1, 2-diketones with alkaline hydrogen peroxide. The acyclic mechanism and its application to the basic autoxidation of pyrogallol. J Am Chem Soc 105(15):5035–5040
84. Wheast R (1984) Handbook of chemistry and physics. CRC Press, Boca Raton
85. Buettner GR (1993) The pecking order of free radicals and antioxidants: lipid peroxidation, α-tocopherol, and ascorbate. Arch Biochem Biophys 300(2):535–543
86. Atkins P (1998) Physical Chemistry, 6th edn. Oxford University Press, Oxford
87. Marcus RA (1956) On the theory of oxidation-reduction reactions involving electron transfer. I J Chem Phys 24(5):966–978
88. Raghavan N, Steenken S (1980) Electrophilic reaction of the hydroxyl radical with phenol. Determination of the distribution of isomeric dihydroxycyclohexadienyl radicals. J Am Chem Soc 102(10):3495–3499